Design and Beam Test Results for the 2D Projective sPHENIX Electromagnetic Calorimeter Prototype

***Abstract*—sPHENIX is a future experiment at the Relativistic Heavy Ion Collider with the goal of studying the quark-gluon plasma and further understanding QCD matter and interactions. A 2D projective prototype of the sPHENIX electromagnetic calorimeter (EMCal) was tested at the Fermilab Test Beam Facility in Spring 2018 as experiment T-1044. The energy response of the EMCal was studied as a function of position and input energy. The resolution of the EMCal prototype was obtained after applying a position dependent energy correction and a beam profile correction. The EMCal energy resolution was found to be $\sigma(E)/\langle E\rangle = 3.5(0.1) \oplus 13.3(0.2)/\sqrt{E}$ based on the hodoscope position dependent correction, and $\sigma(E)/\langle E\rangle = 3.0(0.1) \oplus 15.4(0.3)/\sqrt{E}$ based on the cluster position dependent correction. Both of these results meet the requirements of the sPHENIX physics program.**

***Index Terms*—Calorimeters, electromagnetic calorimetry, performance evaluation, prototypes, Relativistic Heavy Ion Collider (RHIC), silicon photomultiplier (SiPM), simulation, "Spaghetti" Calorimeter (SPACAL), super Pioneering High Energy Nuclear Interaction eXperiment (sPHENIX)**

I. Introduction

sPHENIX is a future experiment [1] at the Relativistic Heavy Ion Collider that will elucidate QCD matter and interactions by studying the quark-gluon plasma (QGP) [2]–[6]. The sPHENIX detector is designed to measure the QGP at a variety of length scales using various probes to provide insights into the microscopic properties of the QGP. One such probe are collimated sprays of correlated particles, called jets, that arise from hard scattering interactions between two partons. The energy loss of partons traversing the QGP is of particular interest. sPHENIX will allow for detailed study of flavor dependent energy loss through measurement of heavy flavor tagged jets, as well as open heavy flavor hadrons. To accomplish these measurements, sPHENIX is designed with a tracking system, a calorimeter system with 2π azimuthal acceptance and pseudorapidity coverage of $|\eta| < 1.1$, and the former BaBar solenoid magnet [7]. The calorimeter system consists of an electromagnetic calorimeter and a hadronic calorimeter. The sPHENIX detector will allow for the measurement of jets with transverse momentum as low as 10 GeV, as well as provide the first measurements of hadronic jet reconstruction at RHIC.

The sPHENIX electromagnetic calorimeter (EMCal) is a sampling calorimeter designed to measure electrons, positrons and photons. The EMCal has a coverage of $|\eta| < 1.1$ and $0 < \phi < 2\pi$. The EMCal is segmented into *towers* of size $\Delta\eta \times \Delta\phi = 0.024 \times 0.024$ that set the granularity of the calorimeter. The towers are defined within calorimeter *blocks* that consist of scintillating fibers embedded in a mix of tungsten powder and epoxy. Each block corresponds to a 2×2 array of towers. Each tower is equipped with a lightguide coupled to silicon photomultipliers that collect the light from the fibers. The blocks are distributed in 64 sectors that describe an overall cylindrical geometry concentric with the beamline and centered at the interaction point of the particle collisions. Each side $0 < |\eta| < 1.1$ has 32 sectors distributed evenly in azimuth. Each sector has 24 rows of blocks extending along the beamline, and each row has 4 blocks along ϕ. The blocks are tapered in both η and ϕ, resembling a truncated pyramid, and giving a 2D projective geometry. The blocks are further tilted such that the fibers do not project directly at the interaction point, minimizing channeling and improving energy resolution.

The EMCal prototype is an array of 8×8 calorimeter towers, or 4×4 blocks, centered at $\eta = 1$. The prototype covers a solid angle of $\Delta\eta \times \Delta\phi = 0.2 \times 0.2$. Figure 1 shows a drawing of the EMCal prototype geometry.

A previous 1D projective prototype of the EMCal was tested in 2016 [8]. There are various differences between the 2016 prototype and the 2018 prototype discussed in this paper. One notable difference is the pseudorapidity region covered by the prototypes. While both prototypes corresponded to a slice $\Delta\eta \times \Delta\phi = 0.2 \times 0.2$ of the EMCal, the 2016 prototype was centered at $\eta = 0$ and the 2018 prototype was centered at $\eta = 1$. Another notable difference is the projectivity of the EMCal blocks. The 2016 prototype was only 1D projective (in ϕ), whereas the 2018 prototype is 2D projective (in η and ϕ). The final design that will be implemented in the EMCal will closely follow the design of the 2018 prototype.

II. Prototype Electromagnetic Calorimeter

A. EMCal Block Production

The EMCal blocks were produced by embedding a matrix of scintillating fibers (SciFi) in a mix of epoxy and tungsten powder (W). The blocks are similar to the "Spaghetti Calorimeter" design used in other experiments [9]–[15]. The scintillating fibers are as long as the block and are distributed uniformly across the block's cross section. There is a total of 2668 fibers per block. The towers within a block have an area of approximately $(1.1R_M)^2$, where $R_M \approx 2.3$ cm is the Molière radius. The length of the towers varies with η and it has an approximate value of $20X_0$, where $X_0 \approx 7$ mm is the radiation length. The blocks have, approximately, a density of 9.5 g/cm^3 and a sampling fraction of 2.3%.

The materials used to produce the blocks are listed in Table I along with some of their properties. The blocks were produced at the University of Illinois at Urbana-Champaign following this procedure:

- Scintillating fibers are dropped into mesh screens that hold the fibers in place.

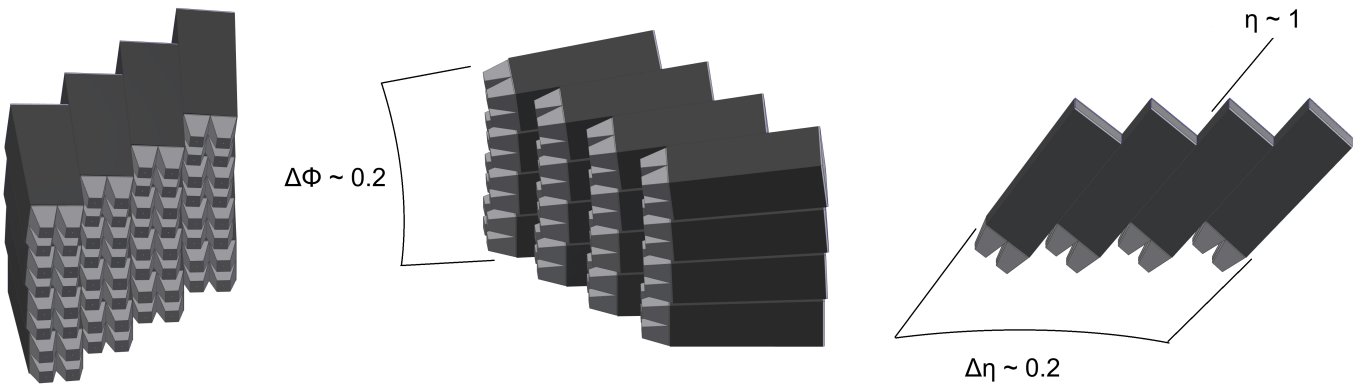

Fig. 1. EMCal prototype. The prototype consists of an array of 4×4 blocks, covering a solid angle of $\Delta\eta \times \Delta\phi = 0.2 \times 0.2$ centered at $\eta = 1$. Each block (dark gray) corresponds to a 2×2 array of towers defined by lightguides (light gray).

- The fiber-screen assembly is put into a mold.
- Tungsten powder is poured into the mold. The mold is placed on a vibrating table to pack the powder.
- Epoxy is poured into the top of the filled mold, while a vacuum pump is used at the bottom to extract the air as well as pull the epoxy through the mold.
- The filled mold is left to dry until the mix is solid.
- The block is unmolded and machined to its final shape. A diamond tip is used to machine the readout ends of the block.

TABLE I
EMCAL BLOCK MATERIALS

Material	Property	Value
Scintillating fiber	Saint Gobain BCF-12	
	diameter	0.47 mm
	core material	polystyrene
	cladding material	acrylic
	cladding	single
	emission peak	435 nm
	decay time	3.2 ns
	attenuation length	$\geq$ 1.6 m
Tungsten powder	THP Technon 100 mesh	
	particle size	25-150 μm
	bulk density (solid)	$\geq$ 18.50 g/cm^3
	tap density (powder)	$\geq$ 10.9 g/cm^3
	purity	$\geq$ 95.4% W
	impurities ($\leq$ 5 percent)	Fe, Ni, O2, Co, Cr, Cu, Mo
Epoxy	EPO-TEK 301	

The finished EMCal block can be seen in Figure 2. The quality assurance of the blocks included tests of density, light transmission and size. The blocks had a density ranging from 9.2 to 9.8 g/cm^3, and all blocks had more than 99% light transmitting fibers. The size of the blocks deviated from the nominal dimensions by less than 0.02 in.

B. Light Collection

The light from the scintillating fibers was collected at the tower's front end (closer to the interaction point). Lightguides were epoxied to the front of the blocks, while aluminum reflectors were epoxied to the back. The lightguides consisted of UV transmitting acrylic with a trapezoidal shape (see Figure 3), custom made by NN, Inc. A silicone adhesive was used to couple each lightguide to an array of 2 × 2 silicon photomultipliers (SiPM) Hamamatsu S12572-33-015P. Each SiPM had 40k pixels distributed evenly in an area of 15×15 μm^2, and a detection efficiency of 25%. The signal per tower was obtained by adding the contribution from each of the four SiPMs. The signal was read by a preamplifier and an amplifier, then shaped and driven into a digitizer. More details about the electronics are given in Section III. Figure 3 shows an EMCal block equipped with lightguides and SiPMs.

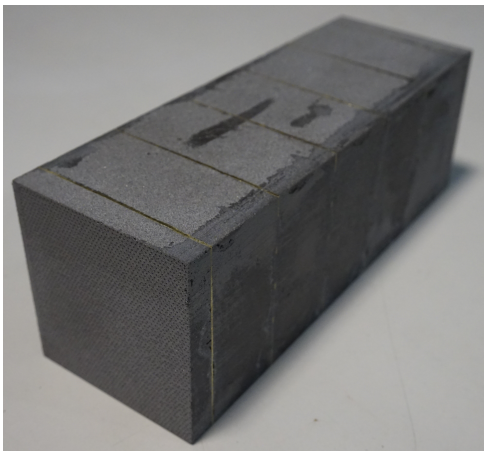

Fig. 2. EMCal block. The block consists on scintillating fibers embedded in a mix of tungsten powder and epoxy. The blocks are tapered in two dimensions, giving a 2D projective geometry.

C. Assembly

Once the EMCal blocks were equipped with lightguides and SiPMs, they were stacked and epoxied together in their final positions. Since the SiPM signal is sensitive to temperature, a cooling system was used to remove the heat generated by the SiPMs and the electronics. The cooling system consisted of multiple water coils connected to cold plates. The plates were coupled to the preamplifier boards that follow the SiPMs. Both the cooling system and electronics were controlled remotely.

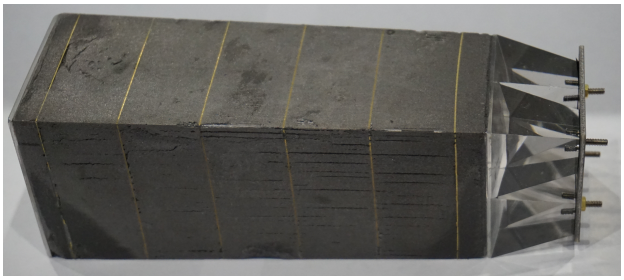

Fig. 3. EMCal block equipped with lightguides and SiPMs.

The EMCal prototype can be seen in Figure 4, which shows the blocks, lightguides, SiPMs, electronics and part of the cooling system.

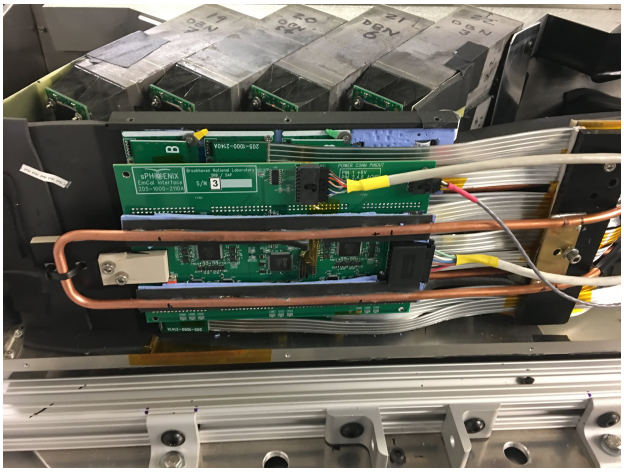

Fig. 4. EMCal prototype showing the SciFi/W blocks, lightguides, SiPMs, electronics and part of the cooling system.

III. Readout Electronics and Data Acquisition

Light was collected in each tower using four SiPMs. The SiPMs voltage was set to have a nominal gain of approximately 2.3×10^5. A small thermistor was mounted at the center of the four SiPMs to monitor the temperature per tower. SiPM signals corresponding to one tower were summed, preamplified, amplified and shaped before going into digitizers. LEDs of 405 nm were included near the front end of the towers to test the SiPMs and preamplifier with fixed amplitude pulses. Similarly, charge injection circuits were included in the amplifiers to provide fixed amplitude pulses for testing. The EMCal prototype could operate in a normal gain mode, or a high gain mode with 16 times the normal gain. The gain was selected through a slow control system.

The slow control system consisted of an interface board connected to a controller board. The interface board was mounted on the EMCal prototype while the controller board was in a separate crate. The interface board contained digital-to-analog converters needed for different testing and monitoring tasks. The interface board controlled SiPM bias and amplifier gain. Testing of preamplifiers and amplifiers was controlled through the interface board as well. The interface board also monitored leakage current and local temperature for compensation. The parameters for these testing and monitoring tasks were provided to the interface board by the controller board. An ethernet connection was used to communicate with the controller board.

Signals were digitized following the trigger using a digitization system developed for PHENIX [16]. Signals were digitized using an analog-to-digital converter (ADC) and Field Programmable Gate Arrays (FPGA). Signals were collected in Data Collection Modules (DCM) and data was finally recorded using the data acquisition system RCDAQ.

IV. Test Beam

The EMCal prototype was tested at the Fermilab Test Beam Facility as experiment T-1044. The facility provided a particle beam, detectors such as a lead-glass calorimeter and a Cherenkov counter, and a motion table (MT6.2C) [17]. The EMCal was placed in the motion table to allow testing in different positions with respect to the beam.

The particle beam used in the experiment had energies ranging from 2 to 28 GeV and a profile size of a few centimeters, dependent on beam energy. The beam was composed mainly of electrons, muons and pions, and their relative abundance depended on the energy [18], [19]. The beam hit the EMCal prototype with a frequency of 1 spill per min, where a spill corresponds to a maximum of approximately 10^5 particles during $4s$. The beam had a nominal momentum spread of $\delta p/p \approx 2\%$ for the energy range used [8], [9], [20]. A lead-glass calorimeter was used to measure the accuracy and precision of the beam momentum. The lead-glass calorimeter had a size of $45 \times 15 \times 15$ cm^3 and a resolution of $(5.6 \pm 0.2)\%/\sqrt{E}$ [21].

External detectors were used to discriminate electron signals from background from minimum ionizing particles (MIPs) and hadrons. A gaseous Cherenkov counter was placed upstream of the EMCal to trigger on electron signals. A hodoscope [9], [10] was placed upstream of the EMCal to determine the position of the particles in the beam precisely. The hodoscope consisted of 16 hodoscope fingers (0.5 cm wide scintillators) arranged in two arrays of 8 fingers each. One array had the hodoscope fingers arranged vertically and the other array had them arranged horizontally. The position of a hit in the hodoscope was given by a horizontal and a vertical hodoscope finger. Each hodoscope finger was read out by an SiPM. Four veto detectors were also placed around the EMCal in order to suppress particles traveling outside the beam position. Each veto counter consisted of a scintillator coupled to a photomultiplier tube (PMT) and read out by a digitizer.

V. Simulations

The EMCal prototype was simulated using GEANT4 [22], [23] version 4.10.02-patch-02. The physics configuration QGSP_BERT_HP was used, which is recommended for high energy simulations. The simulations included an electron beam with an energy between 2 and 28 GeV and a Gaussian profile with an approximate sigma of 3.5 cm. The beam was pointed between Towers 36 and 29, which are located near the center of the prototype (see Figure 5), fully covering the towers. In

the simulations, the energy deposits from the electromagnetic showers were converted into light using Birk's law [24] with constant $k_B = 0.0794$ mm/MeV [25]. The number of photons was converted to number of fired SiPM pixels taking into account the lightguide collection efficiency. The number of fired pixels was converted to ADC counts and then calibrated to energy. To account for SiPM saturation, the energy was reduced by a factor obtained from a Monte Carlo simulation of the SiPMs. The simulations were integrated into the sPHENIX analysis framework.

VI. Analysis Methods

A. Data Sets

The data sets used in this analysis correspond to a beam of electrons with energies of 2, 3, 4, 6, 8, 12, 16, 20, 24 and 28 GeV. The beam was pointed at either Tower 36 or Tower 29 (see Figure 5). In this paper, whenever Tower 36 or Tower 29 is mentioned, it is referring to the corresponding data set that had the beam centered at either of those towers.

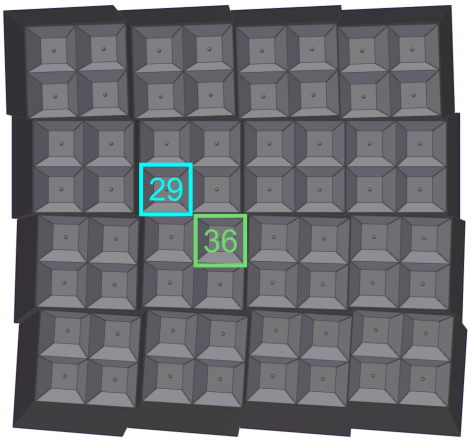

Fig. 5. Front view of the EMCal prototype showing the towers. Tower 36 (light green) and Tower 29 (light blue) are highlighted.

B. Electron Selection

Different cuts were used in order to suppress background from MIPs and hadrons, and select only events with *good* electrons. For an event to be considered a good electron, it had to pass a Cherenkov cut, a vertical and horizontal hodoscope cut, and four veto cuts. For the Cherenkov cut, the energy of the events had to be greater than a threshold of approximately 1500 ADC counts, based on the Cherenkov's energy spectrum. For the vertical and horizontal hodoscope cuts, the events were required to have an energy greater than 50% of the peak energy in the hodoscope's energy spectrum. Only events with one hit in the vertical and one hit in the horizontal hodoscope fingers were considered. For the four veto cuts, the events were required to have an energy less than 20% of the peak energy in the veto's energy spectrum. These cuts gave a number of good electrons of approximately 5000-50000, depending on the energy.

C. Calibration

A preliminary calibration of the data, the *shower calibration*, was performed based on how the electromagnetic showers develop within the EMCal. A uniformity study of the EMCal prototype showed that the energy measurements depend on the position within the EMCal. Figure 6 shows the cluster energy as a function of position for an input energy of 8 GeV, for both data and simulations. A higher energy collection efficiency is observed towards the center of the towers than at the boundaries between blocks and towers. This behavior motivated the use of secondary energy calibrations, the *position dependent correction* and the *beam profile correction*.

The calibration procedures are as follows:

1) Shower calibration: Calibration constants were applied tower-by-tower to convert the ADC signals to energy. For each event, the energy measured by the EMCal was obtained as the total energy of a 5×5 cluster of towers around the maximum energy tower. The size of the cluster was selected based on the Moliére radius for the EMCal blocks. A cluster of 5×5 towers contains over 95% of the shower. The energy corresponding to a cluster of 5×5 towers around the tower with the maximum energy is denoted as E_{cluster}.

2) Position dependent correction: The energy measured by the EMCal was corrected by a constant that depends on the position of the hit in the EMCal. Two different corrections were obtained. In the first one, the position was determined by a horizontal and a vertical hodoscope finger, with a total of 8×8 possible positions. In the second one, the position was determined by the energy averaged cluster position measured by the EMCal, discretized in 8×8 bins that match the hodoscope. The position dependent calibration constants were obtained from 8 GeV data. The procedure is the same for both the hodoscope-based and cluster-based corrections. For each of the 64 possible positions, a histogram was filled with the cluster energy in that position. The histogram was then fit with a Gaussian of mean μ. The calibration constant for each position was obtained as 8 GeV/μ. The position dependent correction improved the energy resolution by 2-3 %, depending on the energy.

3) Beam profile correction: In the experiment, the beam was collimated and had a different profile at different energies. In addition to the position dependent correction, a *beam profile correction* was introduced in order to correct for the energy dependence of the beam profile. This correction consisted on filling the energy histograms with weights that were obtained by uniforming the distribution of beam particles as a function of position. The beam profile correction changed the energy resolution by 0.1-0.5 %, depending on the energy.

The effects of these corrections on the energy response can be seen in Figure 7. This figure shows the cluster energy as a function of horizontal hodoscope position. The data is shown before and after applying the hodoscope-based position dependent correction and the beam profile correction. After the corrections are applied, the energy response of the EMCal becomes more uniform.

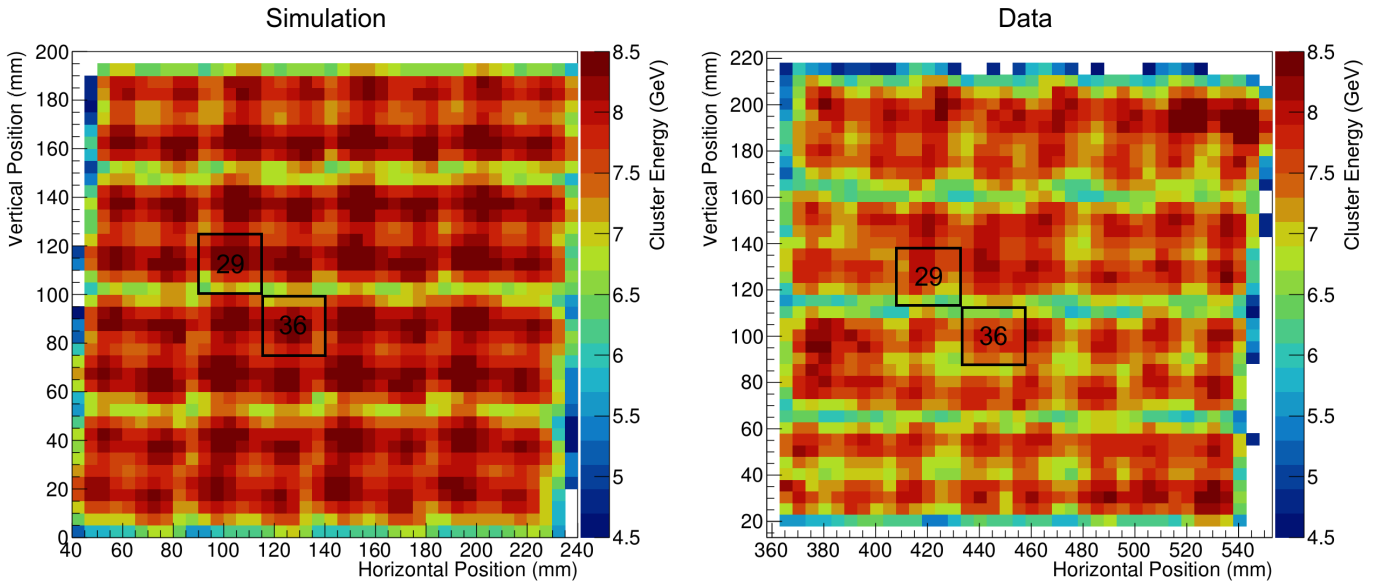

Fig. 6. Cluster Energy vs. Position for simulations (left panel) and data (right panel). The results correspond to an input energy of 8 GeV. Towers 29 and 36 are shown in black squares.

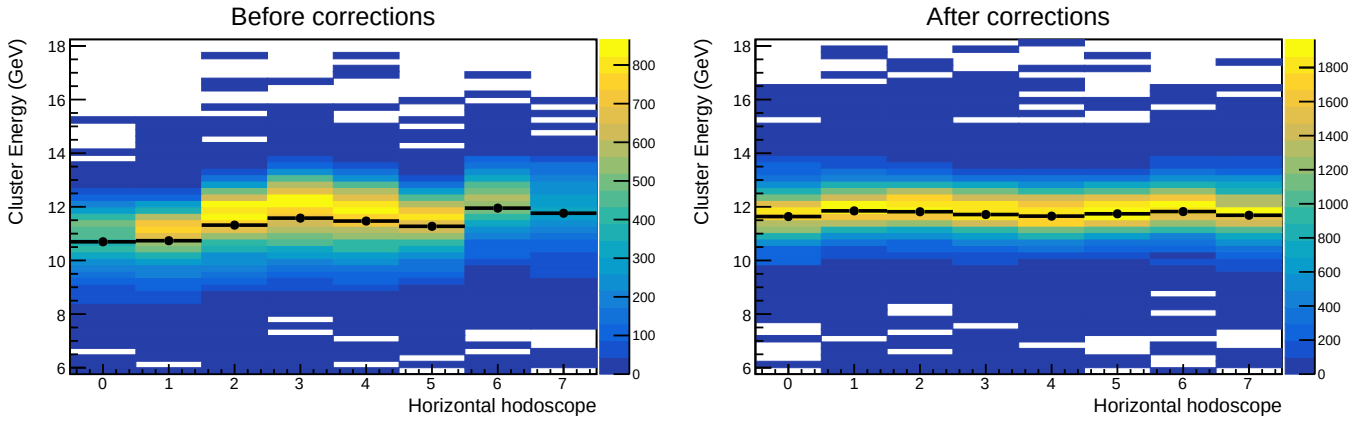

Fig. 7. Cluster Energy vs. Horizontal Hodoscope Position before (left panel) and after (right panel) applying the hodoscope-based position dependent correction and the beam profile correction. The color scale represents the number of events, while the black points correspond to the mean of the energy distributions for each hodoscope position. The data corresponds to a beam of 12 GeV centered at Tower 36.

VII. Results and Discussion

Following the analysis procedure described in the previous section, the energy resolution and linearity of the EMCal prototype was obtained for input energies ranging from 2 to 28 GeV, for both simulations and data.

Figure 8 shows the energy resolution and linearity of the EMCal prototype using a cut of the size of a tower (approximately 2.5×2.5 cm^2) centered at the tower. The results are shown for data and simulations and include all corrections. The uncertainty bars on the data points correspond to the statistical uncertainties. The linearity was obtained as $E_{\rm cluster} = E + cE^2$, where E is the input energy and c is a constant. The resolution was obtained as $\sigma(E_{\rm cluster})/\langle E_{\rm cluster}\rangle = \delta p/p \oplus a \oplus b/\sqrt{E}$, where a and b are constants, and a $\delta p/p = 2\%$ term was added to account for the beam momentum spread. Table II shows the values of the fit constants a, b and c.

TABLE II
EMCal Linearity and Resolution for a 2.5×2.5 cm^2 cut centered on a tower

Resolution fit: $\sigma(E_{\rm cluster})/\langle E_{\rm cluster}\rangle = 2\% \oplus a \oplus b/\sqrt{E}$

Linearity fit: $E_{\rm cluster} = E + cE^2$

	Tower	a	b ($GeV^{1/2}$)	c (GeV^{-1})
Data, hodoscope	36	3.2 ± 0.1	13.8 ± 0.2	(-9.4 ± 0.1)×10^{-4}
Data, hodoscope	29	3.8 ± 0.1	12.8 ± 0.2	(-10.9 ± 0.1)×10^{-4}
Data, cluster	36	2.7 ± 0.1	15.8 ± 0.3	(-12.8 ± 0.2)×10^{-4}
Data, cluster	29	3.2 ± 0.1	14.9 ± 0.3	(-8.6 ± 0.3)×10^{-4}
Simulation		3.04 ± 0.05	12.6 ± 0.1	(-9.3 ± 0.1)×10^{-4}

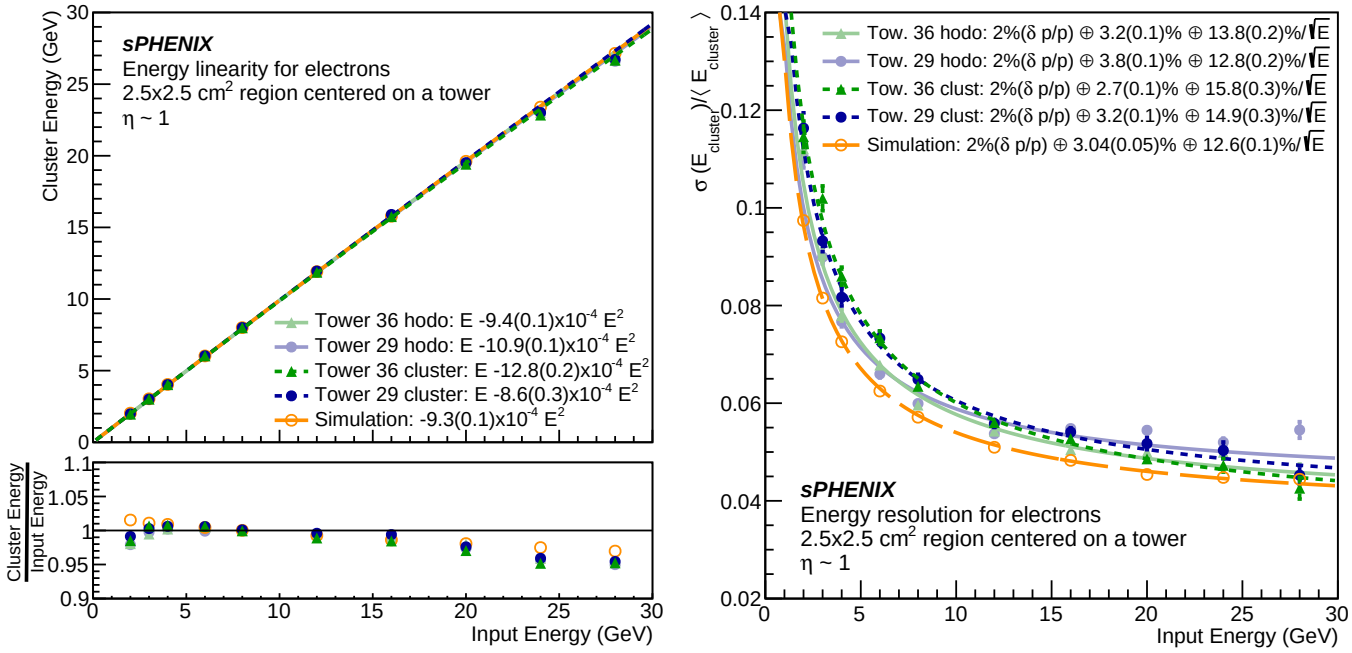

Fig. 8. Linearity and resolution of the EMCal prototype for a 2.5×2.5 cm^2 centered on a tower. The data corresponds to Tower 36 (green triangles) and Tower 29 (purple full circles). The data was corrected using the hodoscope-based (solid lines) and cluster-based (fine dashed lines) position dependent corrections. Simulations (orange open circles, coarse dashed line) are shown for comparison. (top left panel) Cluster Energy vs. Input Energy. (bottom left panel) $\frac{\text{Cluster Energy}}{\text{Input Energy}}$ vs. Input Energy. The linearity was obtained as $E_{\text{cluster}} = E + cE^2$. (right panel) Energy Resolution vs. Input Energy. The resolution was obtained as $\sigma(E_{\text{cluster}})/\langle E_{\text{cluster}}\rangle = \delta p/p \oplus a \oplus b/\sqrt{E}$, where a $\delta p/p = 2\%$ term was added to account for the beam momentum spread.

Figure 8 shows good agreement between towers in terms of linearity and resolution, for both the hodoscope-based and cluster-based position dependent corrections. However, the resolution obtained with the cluster-based correction differs from the hodoscope-based correction by approximately 0.6% in the constant term and 2.1% in the $1/\sqrt{E}$ term. Since the cluster based correction depends on the position measured by the EMCal itself and not the hodoscope, the difference in the results can potentially arise from the cluster position resolution of the EMCal. Additionally, the energy resolution seems to be better in the simulations than in the hodoscope corrected data by approximately 0.5% in the constant term and 0.7% in the $1/\sqrt{E}$ term. These differences can arise from the lower energy collection at the boundaries between towers and blocks, as well as tower by tower variations that are not present in the simulations. The differences in the resolution results can be minimized by making a cut at the center of the towers, where the energy collection is most efficient. Figure 9 shows the linearity and resolution results using a 0.5×1.0 cm^2 cut at the center of the towers. This figure shows better agreement between data and simulations. Table III shows the corresponding linearity and resolution fit constants.

Comparing the 2018 results to the 2016 results of reference [8], the resolution improved for energies in the range 2 to 8 GeV. In terms of the resolution fit, the $1/\sqrt{E}$ term of the resolution decreased by approximately 2.5% and the constant term increased by approximately 0.65%. Furthermore, linearity improved by approximately 1% in the 2018 prototype with respect to the 2016 prototype.

TABLE III
EMCAL LINEARITY AND RESOLUTION FOR A 1.0×0.5 cm^2 CUT AT THE CENTER OF A TOWER

Resolution fit: $\sigma(E_{\text{cluster}})/\langle E_{\text{cluster}}\rangle = 2\% \oplus a \oplus b/\sqrt{E}$

Linearity fit: $E_{\text{cluster}} = E + cE^2$

	Tower	a	b $(GeV^{1/2})$	c (GeV^{-1})
Data, hodoscope	36	2.4 ± 0.2	12.3 ± 0.5	(-12.9 ± 0.3)×10^{-4}
Data, hodoscope	29	2.3 ± 0.2	13.4 ± 0.5	(+0.7 ± 0.3)×10^{-4}
Data, cluster	36	2.4 ± 0.2	13.2 ± 0.5	(-10.9 ± 0.3)×10^{-4}
Data, cluster	29	2.7 ± 0.2	12.8 ± 0.4	(-5.9 ± 0.3)×10^{-4}
Simulation		2.6 ± 0.2	11.9 ± 0.3	(-9.1 ± 0.3)×10^{-4}

VIII. CONCLUSIONS

A 2D projective prototype of the sPHENIX EMCal was constructed and tested. The energy response of the prototype was studied as a function of position and energy. The energy resolution and linearity of the EMCal prototype were obtained using two different position dependent energy corrections (hodoscope-based and cluster-based) as well as a beam profile correction. The two data sets used in this analysis had beam

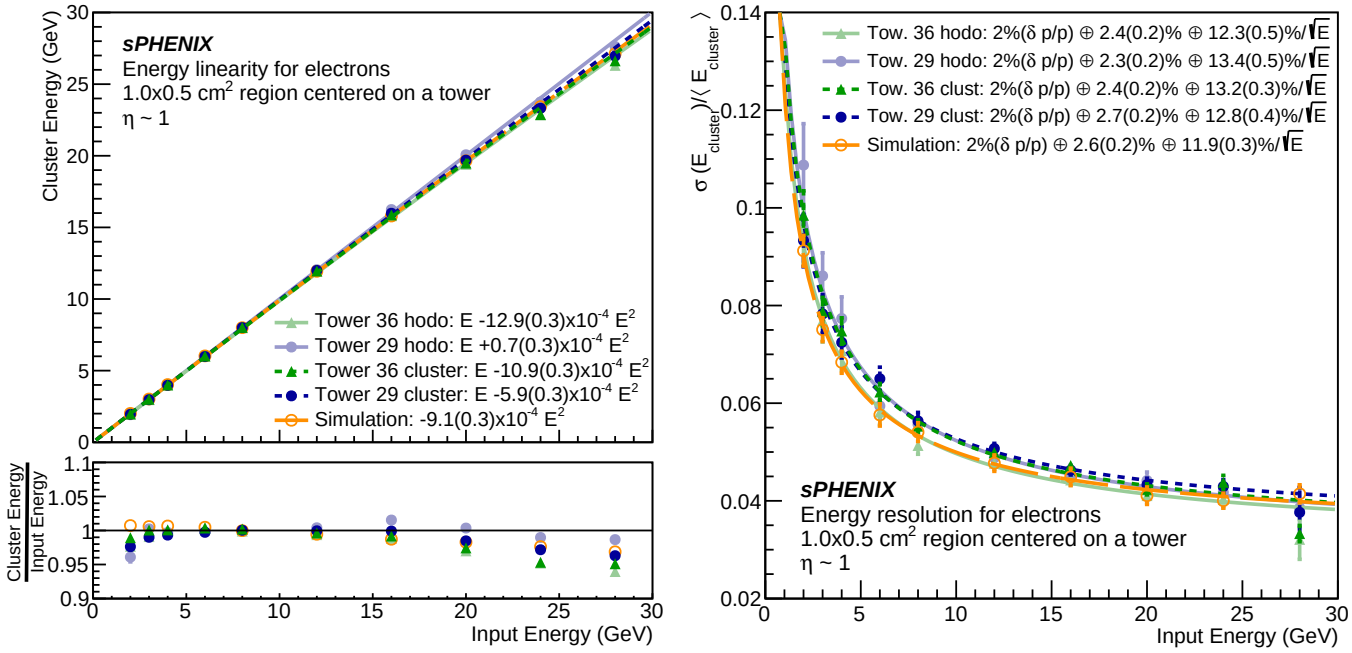

Fig. 9. Linearity and resolution of the EMCal prototype for a 1.0×0.5 cm^2 cut at the center of a tower. The data corresponds to Tower 36 (green triangles) and Tower 29 (purple full circles). The data was corrected using the hodoscope-based (solid lines) and cluster-based (fine dashed lines) position dependent corrections. Simulations (orange open circles, coarse dashed line) are shown for comparison. (top left panel) Cluster Energy vs. Input Energy. (bottom left panel) $\frac{\text{Cluster Energy}}{\text{Input Energy}}$ vs. Input Energy. The linearity was obtained as $E_{\text{cluster}} = E + cE^2$. (right panel) Energy Resolution vs. Input Energy. The resolution was obtained as $\sigma(E_{\text{cluster}})/\langle E_{\text{cluster}}\rangle = \delta p/p \oplus a \oplus b/\sqrt{E}$, where a $\delta p/p = 2\%$ term was added to account for the beam momentum spread.

energies ranging from 2 GeV to 28 GeV, but one had the beam centered at Tower 36 and the other one had the beam centered at Tower 29. The energy resolution was obtained for each tower using a cut of 2.5×2.5 cm^2 centered on the tower. Based on the hodoscope position dependent correction, the EMCal prototype was found to have a tower averaged energy resolution of $\sigma(E)/\langle E\rangle = 3.5(0.1) \oplus 13.3(0.2)/\sqrt{E}$. Based on the cluster position dependent correction, the tower averaged resolution was found to be $\sigma(E)/\langle E\rangle = 3.0(0.1) \oplus 15.4(0.3)/\sqrt{E}$. Both of these results meet the requirements of the sPHENIX physics program.

References

[1] A. Adare *et al.*, "An Upgrade Proposal from the PHENIX Collaboration," 2015.

[2] E.-C. Aschenauer *et al.*, "The RHIC Cold QCD Plan for 2017 to 2023: A Portal to the EIC," 2016.

[3] K. Adcox *et al.*, "Formation of dense partonic matter in relativistic nucleus nucleus collisions at RHIC: experimental evaluation by the PHENIX collaboration," *Nucl. Phys.*, vol. A757, pp. 184–283, 2005.

[4] J. Adams *et al.*, "Experimental and theoretical challenges in the search for the quark gluon plasma: the STAR collaboration's critical assessment of the evidence from RHIC collisions," *Nucl. Phys.*, vol. A757, pp. 102–183, 2005.

[5] B. B. Back *et al.*, "The PHOBOS perspective on discoveries at RHIC," *Nucl. Phys.*, vol. A757, pp. 28–101, 2005.

[6] I. Arsene *et al.*, "Quark gluon plasma and color glass condensate at RHIC? The perspective from the BRAHMS experiment," *Nucl. Phys.*, vol. A757, pp. 1–27, 2005.

[7] T. G. O'Connor *et al.*, "Design and testing of the 1.5 T superconducting solenoid for the BaBar detector at PEP-II in SLAC," *IEEE Trans. Appl. Supercond.*, vol. 9, pp. 847–851, 1999.

[8] C. A. Aidala *et al.*, "Design and Beam Test Results for the sPHENIX Electromagnetic and Hadronic Calorimeter Prototypes," *IEEE Trans. Nucl. Sci.*, vol. 65, no. 12, pp. 2901–2919, 2018.

[9] O. Tsai, L. Dunkelberger, C. Gagliardi, S. Heppelmann, H. Huang *et al.*, "Results of R&D on a new construction technique for W/ScFi Calorimeters," *J. Phys. Conf. Ser.*, vol. 404, p. 012023, 2012.

[10] O. D. Tsai *et al.*, "Development of a forward calorimeter system for the STAR experiment," *J. Phys. Conf. Ser.*, vol. 587, no. 1, p. 012053, 2015.

[11] B. D. Leverington *et al.*, "Performance of the prototype module of the GlueX electromagnetic barrel calorimeter," *Nucl. Instrum. Meth.*, vol. A596, pp. 327–337, 2008.

[12] S. A. Sedykh *et al.*, "Electromagnetic calorimeters for the BNL muon (g-2) experiment," *Nucl. Instrum. Meth.*, vol. A455, pp. 346–360, 2000.

[13] T. Armstrong *et al.*, "The E864 lead-scintillating fiber hadronic calorimeter," *Nucl. Instrum. Meth.*, vol. A406, pp. 227–258, 1998.

[14] R. D. Appuhn *et al.*, "The H1 lead / scintillating fiber calorimeter," *Nucl. Instrum. Meth.*, vol. A386, pp. 397–408, 1997.

[15] D. W. Hertzog, P. T. Debevec, R. A. Eisenstein, M. A. Graham, S. A. Hughes, P. E. Reimer, and R. L. Tayloe, "A high resolution lead scintillating fiber electromagnetic calorimeter," *Nucl. Instrum. Meth.*, vol. A294, pp. 446–458, 1990.

[16] W. Anderson *et al.*, "Design, Construction, Operation and Performance of a Hadron Blind Detector for the PHENIX Experiment," *Nucl. Instrum. Meth.*, vol. A646, p. 35, 2011.

[17] The Fermilab test beam facility. accessed: Apr 5, 2017. [Online]. Available: http://ftbf.fnal.gov

[18] N. Feege, "Low-energetic hadron interactions in a highly granular calorimeter," Ph.D. dissertation, Physics Department, Hamburg U., 2011. [Online]. Available: http://www-library.desy.de/cgi-bin/showprep.pl?thesis11-048

[19] M. Blatnik *et al.*, "Performance of a Quintuple-GEM Based RICH Detector Prototype," *IEEE Trans. Nucl. Sci.*, vol. 62, no. 6, pp. 3256–3264, 2015.

[20] M. Backfish, "Meson test beam momentum selection," http://beamdocs.fnal.gov/AD/DocDB/0048/004831/004/DPoverP.pdf, 2016.

[21] R. M. Brown, W. M. Evans, C. N. P. Gee, P. W. Jeffreys, G. N. Patrick, M. D. Rousseau, B. J. Saunders, and M. Sproston, "An Electromagnetic

Calorimeter for Use in a Strong Magnetic Field at LEP Based on Ceren 25 Lead Glass and Vacuum Phototriodes," *IEEE Trans. Nucl. Sci.*, vol. 32, pp. 736–740, 1985.

[22] S. Agostinelli *et al.*, "GEANT4: A Simulation toolkit," *Nucl. Instrum. Meth.*, vol. A506, pp. 250–303, 2003.

[23] J. Allison *et al.*, "Geant4 developments and applications," *IEEE Trans. Nucl. Sci.*, vol. 53, p. 270, 2006.

[24] J. B. Birks, "Scintillations from Organic Crystals: Specific Fluorescence and Relative Response to Different Radiations," *Proc. Phys. Soc.*, vol. A64, pp. 874–877, 1951.

[25] M. Hirschberg, R. Beckmann, U. Brandenburg, H. Brueckmann, and K. Wick, "Precise measurement of Birks k_B parameter in plastic scintillators," *IEEE Trans. Nucl. Sci.*, vol. 39, pp. 511–514, 1992.